Traffic 2009; **10:** 894–911

doi: 10.1111/j.1600-0854.2009.00910.x

The Single ENTH-Domain Protein of Trypanosomes; Endocytic Functions and Evolutionary Relationship with Epsin

Carme Gabernet-Castello[1], Joel B. Dacks[1,2] and Mark C. Field[1,*]

[1]Department of Pathology, University of Cambridge, Tennis Court Road, Cambridge, CB2 1QP, UK
[2]Department of Cell Biology, University of Alberta, 6-30 Medical Science Building, Edmonton, Alberta, Canada
**Corresponding author: Mark C. Field, mcf34@cam.ac.uk*

Epsin N-terminal homology (ENTH) domains occur in proteins of either the epsin or epsin-related (epsinR) form. They principally function in clathrin-mediated trafficking and membrane deformation. Both epsin and epsinR possess clathrin-binding motifs, but only epsin incorporates a ubiquitin-interaction motif (UIM). To better understand the origins of ENTH-domain proteins and their functions, we performed detailed comparative genomics and phylogenetics on the epsin family. The epsin ENTH-UIM configuration is an architecture restricted to yeast and animals. Further, we undertook functional analysis in *Trypanosoma brucei (T. brucei)*, a divergent organism possessing a single ENTH-domain protein (TbEpsinR). TbEpsinR has a cellular location similar to both epsin and epsinR at plasma membrane clathrin budding sites and endosomal compartments, and associates with clathrin, as demonstrated by coimmunoprecipitation. Knockdown of TbEpsinR leads to a significant decrease in the intracellular pools of multiple surface antigens, without affecting bulk membrane internalization. Therefore, despite lacking the UIM, TbEpsinR maintains a similar role to metazoan epsin in endocytosis and participates as a clathrin-associated adaptor. We suggest that recruitment of a UIM to the ENTH-domain proteins was not essential for participation in endocytosis of ubiquitylated molecules, and is presumably a specific innovation restricted to higher eukaryotes.

Key words: endocytosis, ENTH, epsin, trypanosomes, ubiquitylation, vesicle transport

Received 4 September 2008, revised and accepted for publication 5 March 2009, uncorrected manuscript published online 17 March 2009, published online 8 April 2009

Endocytosis is the mechanism by which material at the cell surface is internalized and subsequently sorted. Multiple distinct modes of endocytosis have been described, defined by dependence on various protein factors, e.g. clathrin, caveolin and flotillin (1). Endocytosis is essential for nearly all eukaryotic cells and required for the efficient uptake of nutrients, signal transduction and maintenance of composition of the plasma membrane, amongst other functions (2–5). Several mechanisms have arisen through eukaryotic evolution to mark and sort endocytic cargo proteins. These include linear peptide motifs embedded in the cytoplasmic region of a polypeptide (6) and post-translational signals, in particular phosphorylation, glycosylation and/or ubiquitylation (7). A large number of cytoplasmic factors are required to accurately recognize these various endocytic signals and to drive traffic to the correct destination. Determining the identity and role of these accessory proteins has been the focus of much effort, based primarily in animals and fungi, and has revealed a highly complex network of protein–protein and protein–lipid interactions (8).

One set of clathrin-associated sorting proteins (CLASPs) is defined by the presence of an epsin N-terminal homology (ENTH) domain at the N-terminus, and is named Eps15-interacting proteins (epsin), after a subgroup of this class of alternative adaptors (9). Initial studies in mammalian cells led to the classification of members of the family as epsin or epsin-related (epsinR) based on function [endocytosis of ubiquitylated cargo (epsin), or sorting/recycling of cargo within intracellular compartments (epsinR)], domain architecture [based on the presence of ubiquitin-interacting motif (UIM) within the C-terminus of the sequence (epsin) or not (epsinR)] and cellular location, i.e. plasma membrane or intracellular compartments respectively (10,11). Epsins are involved in endocytosis in both mammals and fungi (9,12). In mammalian systems, a role for epsinR in retrograde transport has been reported (13). In *Arabidopsis*, ENTH proteins are implicated in vacuolar trafficking (14) and transport from the *trans*-Golgi network (TGN) by specifically interacting with SNAREs functioning in vesicle fusion at the TGN (15) as also observed in yeast and mammals (16). In *Dictyostellium,* epsin is reported to directly influence HIP1r (17), a clathrin-associated protein that performs a regulatory role in actin dynamics. The actin cytoskeleton is also a vital component of the endocytic process, regulating both the initial endocytic event by facilitating inward membrane deformation and also participating in subsequent pathways for transport of endocytosed vesicles to intracellular compartments (18). Interestingly, recent work has uncovered an interaction of epsin-like adaptors with factors that regulate the status of the actin cytoskeleton, suggesting a major role in this process (17,19).

From previous comparative genomic analysis it was suggested that the ENTH module is conserved amongst genomes representing all major eukaryotic supergroups (20). A duplication and specialization appeared to have occurred in fungal and metazoan lineages producing the non-redundant epsin and epsinR subtypes, where the major innovation is the inclusion of a UIM, in addition to the common ENTH and clathrin-recognition boxes. The UIM appears essential for sorting of ubiquitylated cargo and potentially is involved in coupling endocytosis to actin dynamics. The bulk of functional information on epsin-like adaptors derives from cell models where both epsin and epsinR coexist. Hence, the question arises as to which roles ascribed to the two types exist in the ancestral ENTH-containing adaptor lacking the UIM, i.e. epsinR, and more significantly, in a lineage where the epsin form has never been present? Comparative genomics also suggests that caveolin-dependent endocytosis is a recent acquisition, restricted to metazoans, while clathrin-dependent endocytosis and associated adaptor complexes are significantly more conserved across the eukaryotes (20). Furthermore, within the endosomal sorting complex required for transport (ESCRT) system, which sorts ubiquitylated cargo, the ESCRT 0 complex appears to be opisthokont specific (21), representing a significant innovation. Non-animal/fungal taxa indeed appear to have less complexity in their repertoire of adaptor proteins, i.e. CLASPs, and other accessory proteins (20).

Trypanosoma brucei (T. brucei) is an extracellular protozoan parasite, belonging to the supergroup Excavata. Consequently trypanosomes are distantly related to the well-studied model organisms of animals and fungi and are thus a tractable organism from which to compare function across deep evolutionary time. To more fully understand the evolution, diversity and functions of the epsin family, we extended our earlier comparative genomic analysis by deeper taxon sampling, using phylogenetics to reconstruct epsin evolutionary history. There is evidence for both lineage-specific epsin architecture, and accessory factors operating with epsins, suggesting a major difference in the mechanisms by which ENTH-domain proteins function in opisthokonts and other taxa. Further, *T. brucei* has a single ENTH-domain epsin-related protein encoded by the genome (Tb11.50.0006), which we exploited as an opportunity for functional analysis in an evolutionary context. We find that TbEpsinR is essential and functions in clathrin-mediated endocytosis of ubiquitylated cargo despite the lack of conservation in domain architecture found in epsin adaptors.

Results

Phylogenetics and comparative genomics of epsin-like adaptor proteins

ENTH-domain protein sequences were obtained using the basic local alignment search tool (BLAST) from complete genome databases representing the 5 of the 6 recognized eukaryotic supergroups with genomic sampling publicly available; orthology was confirmed by reverse BLAST. Interestingly, while multiple homologues were obtained from metazoa, fungi and *Arabidopsis thaliana (A. thaliana),* most organisms contain only a single unambiguous homologue. Phylogenetic analysis of a dataset encompassing all the putative epsin/epsinR homologues identified lineage-specific expansions in *A. thaliana*, but otherwise little resolution was obtained (supporting information). This was likely due to inclusion of divergent sequences, some of which do not retain all the canonical ENTH-domain features, resulting in poor conservation and long-branch effects. Therefore, a selected dataset containing those sequences with canonical ENTH domains and still representing all five supergroups was analyzed; this reconstructed clades for epsinR homologues from chromalveolates, kinetoplastids, animals and fungi (Figure 1). Importantly, a separate, clade containing exclusively opisthokont lineages, and only the epsins, was also recovered. This result is consistent with the hypothesis that epsinR, rather than epsin, is the ancient and hence more general eukaryotic ENTH-domain protein configuration (20) and suggests that association of the UIM with the ENTH domain is specific to the opisthokonts.

Alignment of selected ENTH domain predicted amino acid sequences demonstrated high levels of conservation across divergent species, with several completely conserved residues (Figure 2A). In most cases, predicted clathrin-binding motifs are retained within this sequence, α-adaptin and γ-adaptin binding short peptide motifs also occur in several sequences (Figure 2B). The number of motifs and their positions varies considerably between species (data not shown). Importantly, the DPW and DFG α-adaptin and γ-adaptin binding motifs are absent from the *T. brucei* TbEpsinR sequence, which may reflect the absence of Golgi-localizing, gamma-adaptin ear domain homology ARF-binding adaptors (GGAs) from non-opisthokont taxa (20) and also the selective secondary loss of AP-2 from African trypanosomes (20).

Most significantly, none of the epsin homologues in the non-opisthokonts harbors the ENTH-UIM domain architecture (Figure 2B). Within the ENTH domain, basic residues that participate in binding to phosphatidylinositol phosphate (PtdInsP) lipids are well conserved. Variations within these residues may reflect altered affinity or PtdInsP specificity (Figure 2C).

TbEpsinR is located at endosomes

Co-evolution of epsin and epsinR within fungi and animals potentially confounds determination of original epsinR function. Hence, we considered a lineage that never possessed epsin and potentially retains the ancestral ENTH-domain family configuration. We chose *T. brucei* for analysis based on a well-characterized endocytic system, including the presence of an endosomal ubiquitylation system (24–26).

Bioinformatic searches identified Tb11.50.0006 on chromosome 11 as the sole ENTH-domain encoding open reading frame (ORF) in *T. brucei*. The predicted gene product is a protein of 55.2 kDa, pI6.5 and a member of the epsinR family (Figures 1 and 2). The ENTH domain of Tb11.50.0006 is 34% identical to both *Homo sapiens*

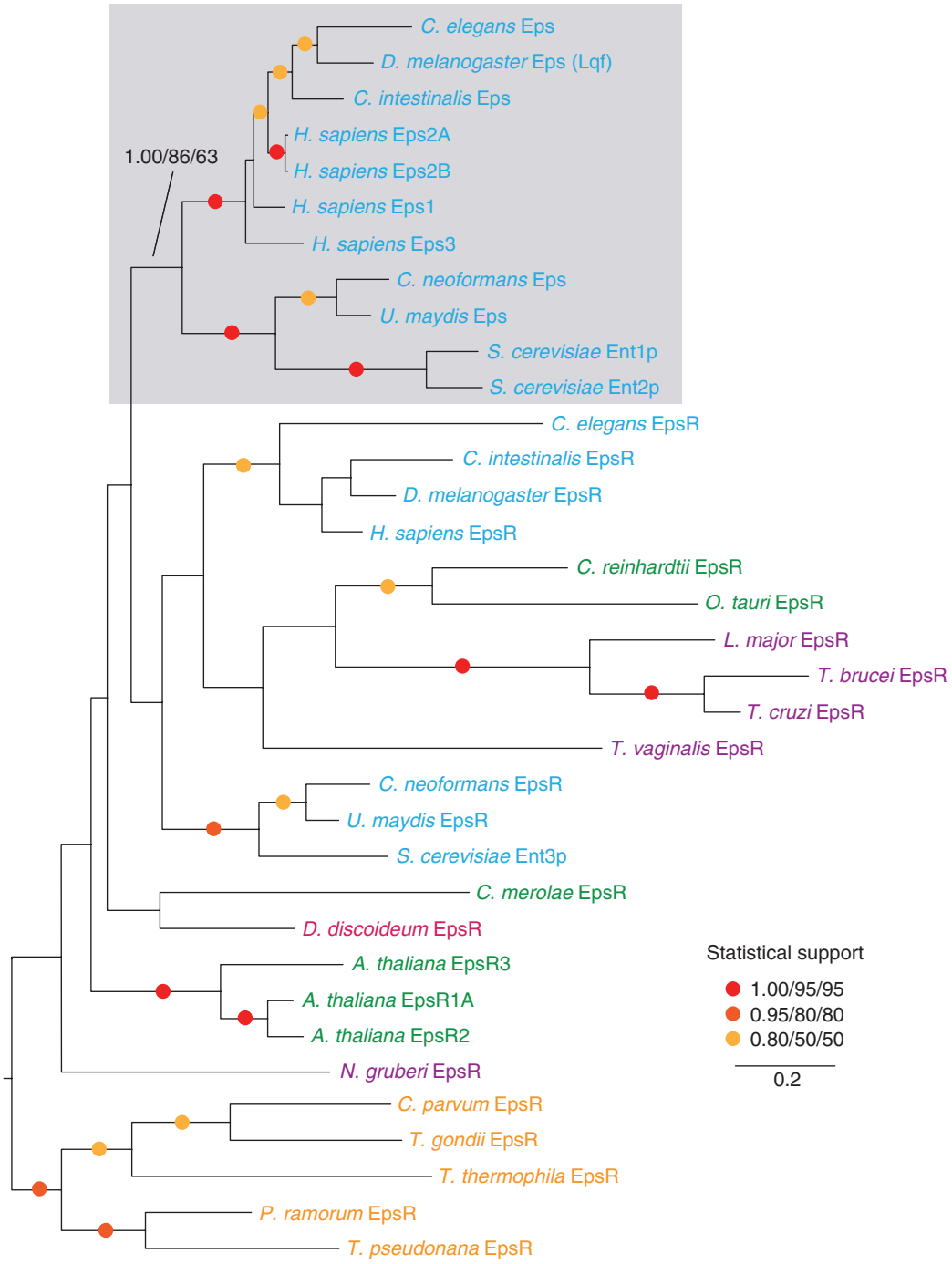

Figure 1: Phylogenetic reconstruction of the epsin ENTH-domain family. Selected completed eukaryotic genomes were searched for ENTH-domain epsin-like proteins (see *Methods*), sequences were aligned, edited for regions of poor alignment and subjected to phylogenetic analysis using Baysian inference and maximum-likelihood methods. The topologies in all cases were identical. Statistical support is shown for important nodes either as raw values or as colored dots—values are Bayesian/PhyML/RaxML. Taxa are color coded for membership of eukaryotic supergroups; Opisthokonta—light blue, Plantae—green, Amoebozoa—pink, Chromalveolata—orange, Excavata—purple. Note that the epsin sequences are all derived from Opisthokonta (shaded), whereas epsinR contains taxa representing all supergroups.

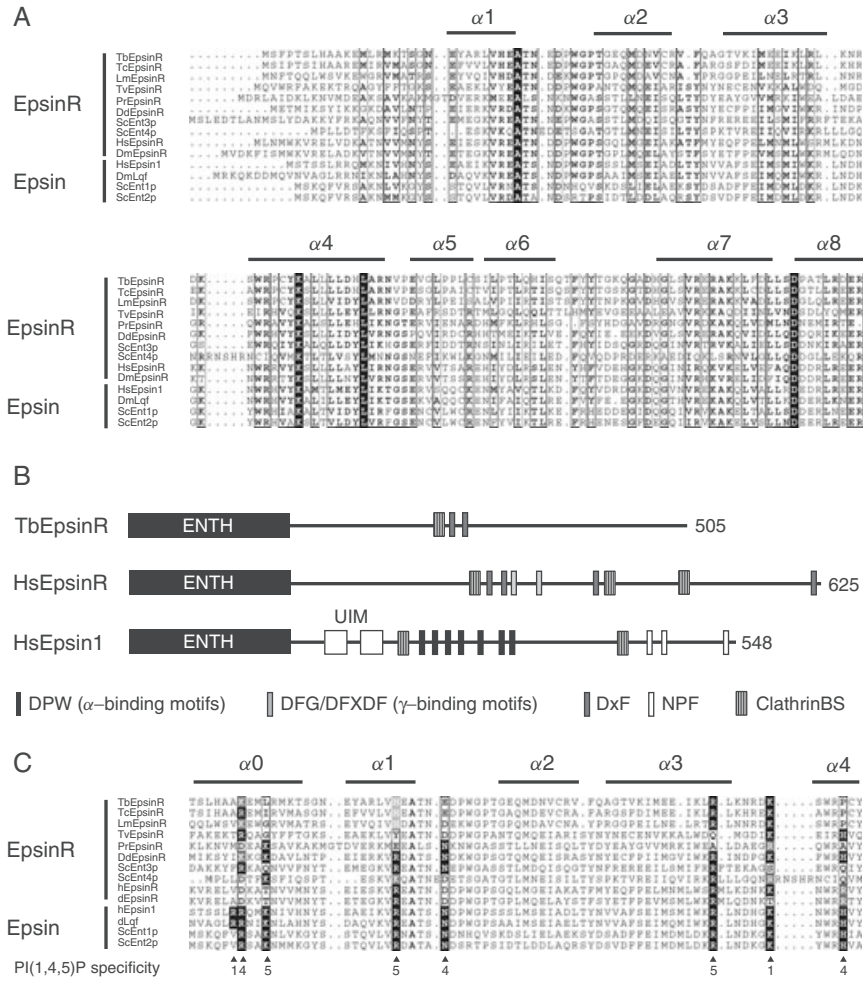

Figure 2: Conservation of ENTH-domain structure and TbEpsinR domain architecture. Panel A: Sequence comparison of ENTH domains in epsin and epsin-related proteins in taxa representative of the main eukaryotic supergroups, based on a ClustalW sequence alignment. The graphic was assembled with Easy Sequencing in Postscript (ESPRIPT) (22). Residues on a black background are strictly conserved, boxed residues are conserved in more than 70% of included sequences. Secondary structure features based on the crystal structure of *H. sapiens* Epsin are shown above the aligned sequences (23). Panel B: Ribbon representations of *H. sapiens* Epsin, *H. sapiens* EpsinR and *T. brucei* EpsinR. The ENTH domain is shown as a black box, ubiquitin-interaction motifs as open boxes and adaptor binding motifs are indicated in black, gray or white. The overall length of the predicted polypeptide is also shown. The carboxy-terminal segments possess very limited homology with the exception of the presence of the clathrin- and adaptin-binding motifs. Panel C: ENTH sequence alignment highlighting differences in the residues defining PtdInsP-binding specificity. Secondary structural elements are indicated as in Panel A, while residues in *H. sapiens* Epsin implicated in the interaction with the phosphate groups in PtdIns(1,4,5)P are highlighted. Color coding is black for conserved residues and gray for semi-conserved residues, boxed residues designate specificity for PtdIns(1,4,5) phosphate headgroups as in HsEpsin. Note that this alignment differs from the optimal global alignment in Panel A.

(*H. sapiens)* epsin and epsinR ENTH domains, but 33% overall to *H. sapiens* epsinR and 26% to *H. sapiens* epsin. Based on these data we designated Tb11.50.0006 as TbEpsinR. While *T. brucei* has a high developmentally regulated endocytic system, spanning alterations in flux of endocytic cargo and expression of several factors, TbEpsinR mRNA is present at near equivalent levels in the mammalian and insect forms (Figure 3) (27,28).

To address expression and location of TbEpsinR at the protein level, we raised polyclonal antibodies in rabbits against a bacterially expressed TbEpsinR- glutathione S-transferase (GST) fusion protein, followed by affinity purification. Western analysis of lysates from bloodstream stage [bloodstream form (BSF)] cells indicated recognition of a single polypeptide that migrated with an apparent molecular weight of ~ 75 kDa (Figure 3A, right panel). While larger than the predicted molecular weight of 55 kDa, *Rattus norvegicus (R. norvegicus)* epsin has an apparent size of ~ 95 kDa on SDS-PAGE despite a predicted 65 kDa molecular weight, suggesting aberrant mobility is a general feature of this family (9). To ensure that the antibody was indeed specific, in light of the anomalous migration on SDS-PAGE this was verified as recognition was competed with soluble recombinant TbEpsinR-GST (Figure S2), and also subsequently by knockdown (Figure 8).

TbEpsinR antibodies recognized structures at the posterior end of the trypanosome cytoplasm in both life stages, between the nucleus and kinetoplast, a location consistent with a role in the endomembrane system (29) (Figure 3A).

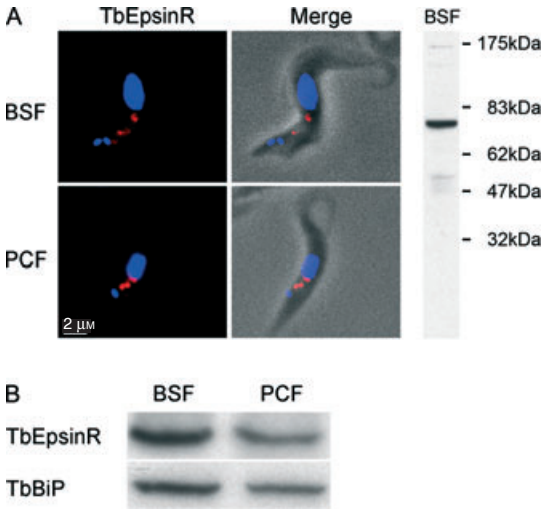

Figure 3: TbEpsinR is expressed at equivalent levels in BSF and PCF trypanosomes, and located to the posterior region of the cell. Panel A: Bloodstream and PCF parasites were fixed and prepared for immunofluorescence analysis using anti-TbEpsinR (red) in BSF (upper panels) and PCF (lower panels), DNA is visualized with 4′,6-diamidino-2-phenylindole (DAPI) (blue). Left; merge of TbEpsinR and DAPI fluorescence. Right; fluorescence channels merged with phase contrast. Extensive staining of membrane structures by TbEpsinR antibody can be observed between the kinetoplast and the nucleus in both life stages. Side panel shows a western blot of BSF cell lysates indicating that a single band is recognized at ~ 75 kDa by the anti-TbEpsinR antibody. Migration positions of molecular weight markers are shown at right. Panel B: TbEpsinR levels in bloodstream and PCFs as assessed by western blot analysis of cell lysates. Membranes were stripped and reprobed with anti-TbBiP to show equivalence of loading. Bars, 2 μM.

Interestingly the intensity of staining appeared rather similar in both stages, and this equivalent expression level was confirmed by western blotting of whole cell lysates (Figure 3B). Although some level of developmental variation in TbEpsinR function cannot be ruled out, we restricted further analyses to the BSF where endocytosis is upregulated and superior molecular markers and assays are available.

TbEpsinR is present on endosomal membranes

To investigate the distribution of TbEpsinR, we conducted a number of immunofluorescence-based analyses using the majority of markers currently available for the trypanosome endocytic pathway. Initially, we stained the endocytic pathway with Concanavalin A-FITC (ConA-FITC). Allowing the cells to accumulate the lectin at 4°C specifically labels the flagellar pocket and at 12°C labels the early endosomes, the latter corresponds to Rab5A-positive compartments (30,31). Cells were counterstained for TbEpsinR. A minor population of TbEpsinR was found in a region in close association with the flagellar pocket (Figure 4A, top panels), but the majority of the population localized to membrane structures that intersect more closely with the early endosome (Figure 4A, middle panels). To investigate the relationship of TbEpsinR to recycling endosomes we costained cells with a combination of TbEpsinR and TbRab11 antibodies. TbEpsinR did not colocalize with the TbRab11 antigen, indicating that TbEpsinR does not have a major presence on recycling endosomes (Figure 4A, bottom panels).

EpsinR adaptors have also been implicated in transport between the TGN and endosomal compartments in metazoans and fungi (13,16,32,33). To investigate possible TbEpsinR presence at the Golgi complex we stained a cell line expressing TbGRASP-GFP with the TbEpsinR antibody. A population of TbEpsinR antibody labeled a membrane domain juxtaposed to TbGRASP-GFP (34) (Figure 4B, top panels), but the staining was clearly distinct, suggesting no significant presence on the trypanosome Golgi apparatus. Finally, to ascertain if TbEpsinR were associated with deep endosomal compartments, we costained cells for TbEpsinR and the lysosomal marker p67 (Figure 4B, bottom panels). No colocalization was observed. Further, we previously reported that TbEpsinR does not colocalize with TbVps28, an ESCRT I component and a marker for the multivesicular body (MVB) (21). Hence TbEpsinR seems to not be associated with the later compartments of the endocytic system that lead to the terminal lysosome and marks an apparently novel subpopulation of structures in trypanosomes.

To extend these studies we performed immunoelectron microscopy on BSF parasites. Consistent with our findings from immunofluorescence, cryosections of bloodstream cells showed the presence of TbEpsinR at internal membrane bounded compartments (Figure 5A, B and E). Occasional gold particles also decorated clathrin-coated membrane both at, and budding from, the flagellar pocket, consistent with the weaker staining seen at the light level near this structure (Figure 5C, D). Significantly, we never found a gold particle on bulk flagellar pocket membrane

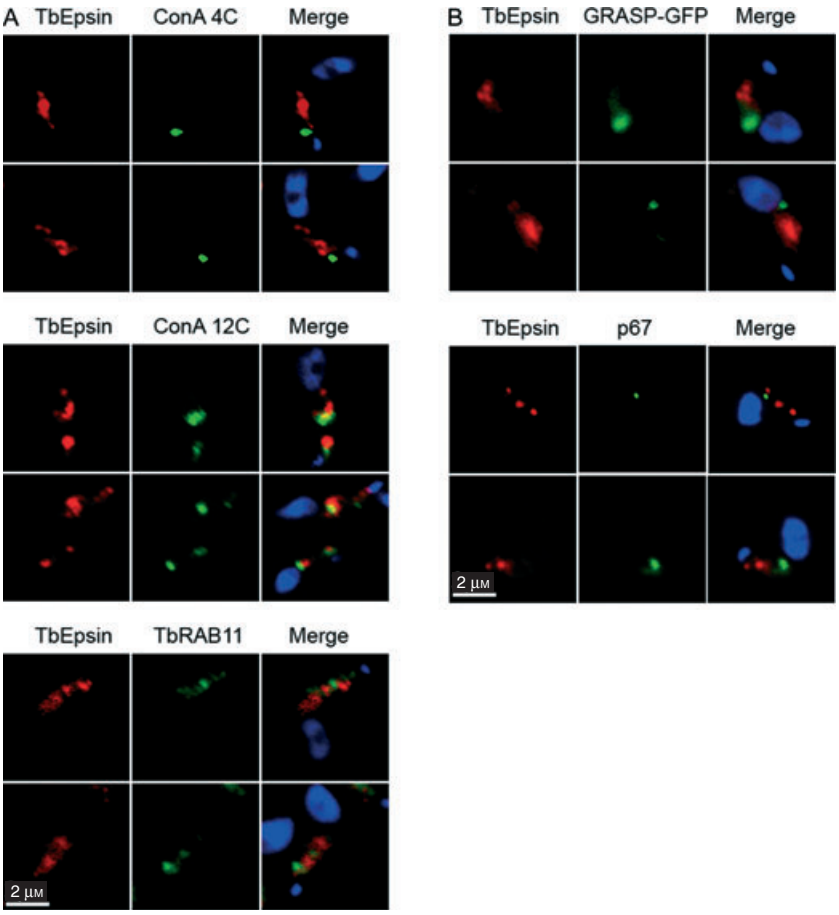

Figure 4: TbEpsinR localizes to distinct endosome-associated compartments. Panel A; top and middle panels: BSF cells were incubated with the lectin Concanavalin A (ConA) (green) at 4°C and 12°C for 20 min to label for the flagellar pocket and early endosomes, cells were then fixed, permeabilized and stained with TbEpsinR antibody (red) and DAPI for DNA (blue). Lower panels; BSF cells were counterstained with TbEpsinR (red) and TbRab11 (green). Panel B; top panels: A BSF strain expressing the Golgi matrix protein TbGRASP, fused to GFP (green), was counterlabeled with TbEpsinR antibody (red). Lower panels; cells were counterstained with TbEpsinR antibody (red) and p67 antibody (green). DNA was visualized with DAPI. Bars, 2 μM.

suggesting an exclusive association with clathrin at this organelle. No staining of electron dense disk-like shape exocytic carriers that recycle endocytosed variant surface glycoprotein (VSG) back to the flagellar pocket was found (35), precluding a major presence on the recycling system, consistent with lack of association with Rab11. Staining with anti-TbEpsinR antibody only ever detected a minority of endosomal compartments, indicating a highly specific and restricted location. These observations are in agreement with the results from the immunofluorescence analysis and indicate that TbEpsinR has a cellular location with similarity to ENTH-domain adaptors of higher eukaryotes.

The ultrastructural data suggest that TbEpsinR has preferential associations with membranes also bearing clathrin, and a putative clathrin-binding box is retained in the TbEpsinR sequence (Figure 2B). We sought to confirm this directly and obtain evidence for a functional connection. The TbEpsinR antibody was used to stain cells expressing the trypanosome clathrin-light chain (CLC) genomically tagged at the C-terminus. Fluorescence microscopy uncovered extensive colocalization between clathrin-associated structures and TbEpsinR (Figure 6A).

To investigate whether clathrin contributes to targeting or binding of TbEpsinR onto the membrane fraction, we use RNAi to knockdown the trypanosome clathrin heavy chain (CLH). Knockdown results in a complete endocytic block with enlargement of the flagellar pocket, the Big Eye morphology (27). We selected for analysis only cells where an enlarged pocket was evident, but prior to onset of gross morphological abnormalities. Knockdown of clathrin resulted in reduction of *T. brucei* clathrin heavy chain (TbCLH) staining as expected (Figure 6B, upper panel). Significantly, reduction of clathrin levels resulted in both decrease of TbEpsinR antibody binding and redistribution of TbEpsinR punctate staining to a diffuse location all over the cell (Figure 6B, lower panels). These data suggest that TbEpsinR requires expression of clathrin for correct targeting to membranes.

To further examine interactions between TbEpsinR and clathrin, we used TbEpsinR and TbCLH antibody to immunoprecipitate TbCLH from lysates of BSF parasites. As specificity controls we used binding protein (BiP) antibody or no antibody. Lysates were added to protein A beads, the beads washed and the presence of bound protein assessed by western blotting. Clathrin was immunoprecipitated together with TbEpsinR. This interaction appears specific as no clathrin could be

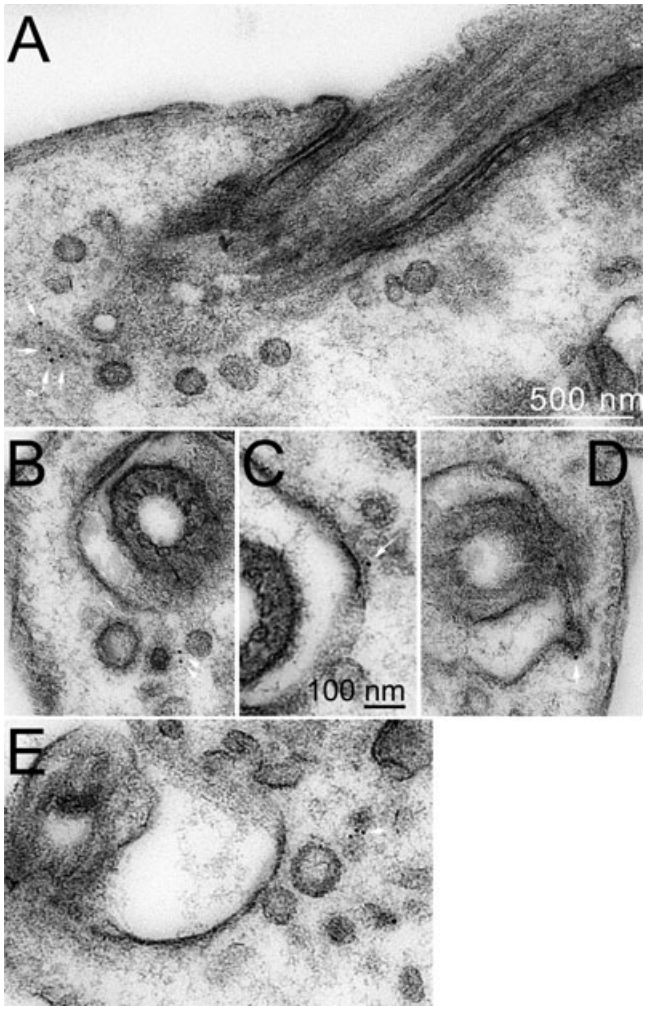

Figure 5: TbEpsinR immunogold electron microscopy. BSF parasites were prepared for immunoelectron microscopy (see *Methods*). Thawed cryosections were stained with affinity-purified anti-TbEpsinR antibody followed by gold-conjugated secondary antibody. Labeling for TbEpsinR was found primarily on the cytoplasmic face of, or in close proximity to, intracellular vesicles (panels A, B and E), clathrin-coated pits budding from the flagellar pocket membrane (panel B) and clathrin-coated areas of the flagellar pocket (panel C). Gold was not observed associated with non–clathrin-coated vesicles associated with the flagellar pocket membrane, indicating no detectable presence at recycling endosomal structures. In all cases only a minority of vesicular structures close to the flagellar pocket were labeled suggesting either selective loading onto vesicles or transient association only. Bar in panel A is 500 nm. Panels B, D and E were taken under the same magnification as panel A. Bar in panel C is 100 nm.

detected in the BiP or no antibody control (Figure 6C). Taken with the ultrastructural evidence, these data suggest that TbEpsinR associates in a complex with clathrin, and that this association is required for faithful targeting to membranes.

Recruitment of TbEpsinR to the membrane is dependent on PtdIns membrane composition

Residues implicated in PtdInsP recognition are retained in TbEpsinR (Figure 2C). To determine if the ENTH domain of TbEpsinR influences membrane targeting of TbEpsinR, we carried out immunofluorescence studies under conditions expected to perturb phosphoinositide lipid synthesis and dephosphorylation. An initial subcellular fractionation using hypotonic lysis of trypanosome cells indicated that TbEpsinR is present at equivalent levels as both cytosolic and membrane-associated populations (Figure 7A).

In *H. sapiens* Rab5 serves as a master regulator for endosomal synthesis of PtdIns(3)P, both *via* recruitment of PI3K-β and Vps34 and of phosphatases that convert higher order PtdInsP lipids to PtdIns(3)P (36). Knock down of TbRab5A resulted in increased intracellular staining of TbEpsinR (Figure 7B, left panels) as quantitated by single cell immunofluorescence analysis of cells that retained a normal morphology (Figure 7C, left). In cells with an enlarged flagellar pocket, TbEpsinR accumulated around the flagellar pocket area on structures that did not correlate to any endocytic vesicles as visualized by electron microscopy (EM) (Figure S3). TbEpsinR levels in TbRab5A knock down cells were increased overall as assessed by western blot analysis of TbRab5A RNAi cells (Figure S4). The role of TbPI4KIII-β in trafficking has been previously characterized (37); Similar to the TbRab5A knockdown, TbEpsinR intracellular staining in an induced TbPI4KIII-β RNAi BSF cell line was increased (Figure 7B and C, middle panels) and resulted in accumulation of TbEpsinR in cells that presented an enlarged flagellar pocket, similar to as observed for TbRab5A RNAi.

To assess whether the increase in TbEpsinR intracellular staining was result of an impairment in PtdIns(3)P synthesis on endosomal membranes we used the PI3K inhibitor wortmannin, previously shown by us to act in a

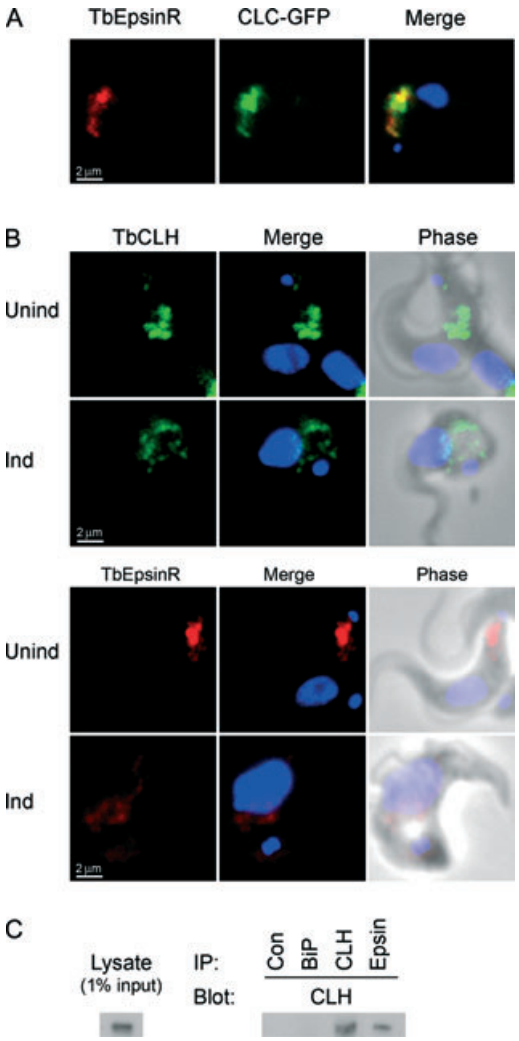

Figure 6: TbEpsinR association with clathrin. Panel A: BSF cells expressing green fluorescent protein (GFP) genomic-tagged (CLC-GFP) (green) were counterstained with anti-TbEpsinR antibody (red). TbEpsinR labeling shows extensive overlap with CLC-GFP. Panel B: RNAi against (TbCLH) was induced with 1 μg mL^{-1} tetracycline for 12 h (+TET). Cells were then fixed and further processed for labeling with anti-TbCLH (green) (upper panels) or anti-TbEpsinR (red) (lower panels) antibodies. TbEpsinR becomes mislocalized in the clathrin knockdown in cells with a Big Eye morphology when compared with uninduced cells (–TET). Cells were counterstained with DAPI to visualize the nucleus and kinetoplast. Panel C: Clathrin heavy chain can be co-immunoprecipitated with anti-TbEpsinR antibody and anti-TbCLH antibody. As specificity controls anti-TbBiP and no antibody (Con) were used. Lysates were probed with affinity-purified antibody to TbCLH. Bars, 2 μM.

similar manner in trypanosomes as in higher eukaryotes (38). BSF cells treated with wortmannin showed no significant increase in membrane-associated TbEpsinR in cells with a normal morphology (Figure 7B and C, right panels), although a small increase in TbEpsinR staining of endosomal structures was, however, observed in cells that presented an enlarged flagellar pocket (Figure 7B). Overall these data suggest an accumulation of intracellular TbEpsinR under circumstances of perturbed phosphoinositide levels (39).

TbEpsinR expression is essential in BSF cells

To directly address the roles of TbEpsinR in endocytosis and membrane trafficking, we used RNAi. Expression of double-stranded RNA from p2T7TbEpsinR in an inducible BSF cell line (40) caused a severe growth defect manifest at early time points of induction (Figure 8A), which correlated with a rapid loss of TbEpsinR protein levels as seen by western blot (Figure 8B) and immunofluorescence (Figure 8C) analysis at 6 and 12 h post induction. Moreover, no effect on expression levels of clathrin, Rab5A, Rab11 or BiP were observed, suggesting that any alterations were specific and not due to secondary effects, as observed, for example, in knockdown of TbRab5A on clathrin expression (41). Furthermore, the locations of clathrin and TbRab5A were unaffected, and suggest that endosome maintenance either does not require TbEpsinR or utilizes multiple

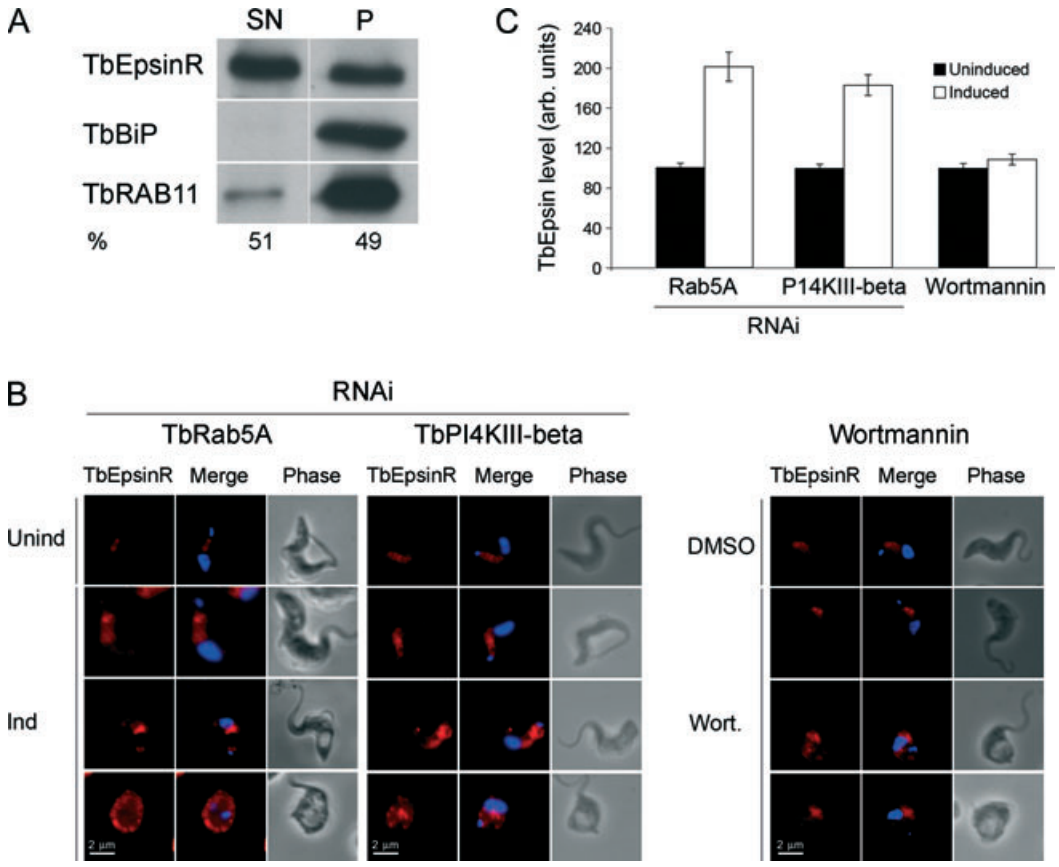

Figure 7: Role of the ENTH-domain and PtdInsP in TbEpsinR localization. Panel A: BSF cells were grown to log-phase and lysed under hypotonic conditions. Supernatant (SN) and pellet (P) fractions were recovered, concentrated to normalize loading and analyzed by western blotting. TbEpsinR is present at equivalent levels as cytosolic and membrane-bound populations (upper panel). As expected, the endoplasmic reticulum (ER) chaperone TbBiP is restricted to the pellet fraction (middle panel), the majority of TbRab11A is in the pellet and a small proportion can also be detected in the SN, consistent with previous work (bottom panel). Panel B: Immunofluorescence detection of TbEpsinR in TbRab5A (left panels), TbPI4KIII-β (middle panels) RNAi cells induced with 1 μg mL^{-1} tetracycline for 24 h and 72 h respectively, and BSF treated with wortmannin 30 μM for 1 h (right panels). Treated cells were fixed and further labeled with anti-TbEpsinR antibody (red). Cells were counterstained with DAPI to visualize the nucleus and kinetoplast. Panel C: Histograms represent quantitation of intracellular immunofluorescence, values are expressed in percentage of treated to untreated and represent mean values of at least $n = 30$ cells. Bars, 2 μM.

and redundant mechanisms that can compensate for the loss of TbEpsinR. These data also indicate that the effects of clathrin knockdown on TbEpsinR location are not reciprocal, suggesting that clathrin acts upstream of TbEpsinR in recruitment to the membrane.

The presence of a significant proportion of the cell population with multiple nuclei and kinetoplasts is indicative of a severe disruption of membrane transport that affects completion of cytokinesis (Figure S5). Finally, the Big Eye enlarged flagellar pocket phenotype was only seen in an extremely small percentage of the population as scored by light microscopy of fixed TbEpsinR RNAi cells at 24 h of induction (Figure S5), suggesting that TbEpsinR does not have a major role in bulk membrane endocytosis, and consistent with the absence of an effect on either clathrin protein levels or localization. An enlarged vacuole, seen in a slightly higher proportion of induced cells compared with controls had neither the morphology nor the correct position for the BigEye (Figure S5). These observations are consistent with a role of TbEpsinR as a transport adaptor, and not a structural component of the endosomal machinery.

TbEpsinR is required for endocytosis of both trans-membrane domain and GPI-anchored surface proteins

To uncover any specific roles of TbEpsinR in endocytosis we measured total and intracellular levels of several well-characterized molecules following TbEpsinR silencing. We included ESAG6/7 transferrin receptor (TfR), and invariant surface glycoproteins ISG65 and ISG75; TfR is a GPI-anchored molecule restricted to the flagellar pocket (42), while ISG65 and ISG75 are *trans*-membrane domain proteins internalized by a ubiquitin and ESCRT-dependent mechanism [(21,26), Leung and MCF unpublished data].

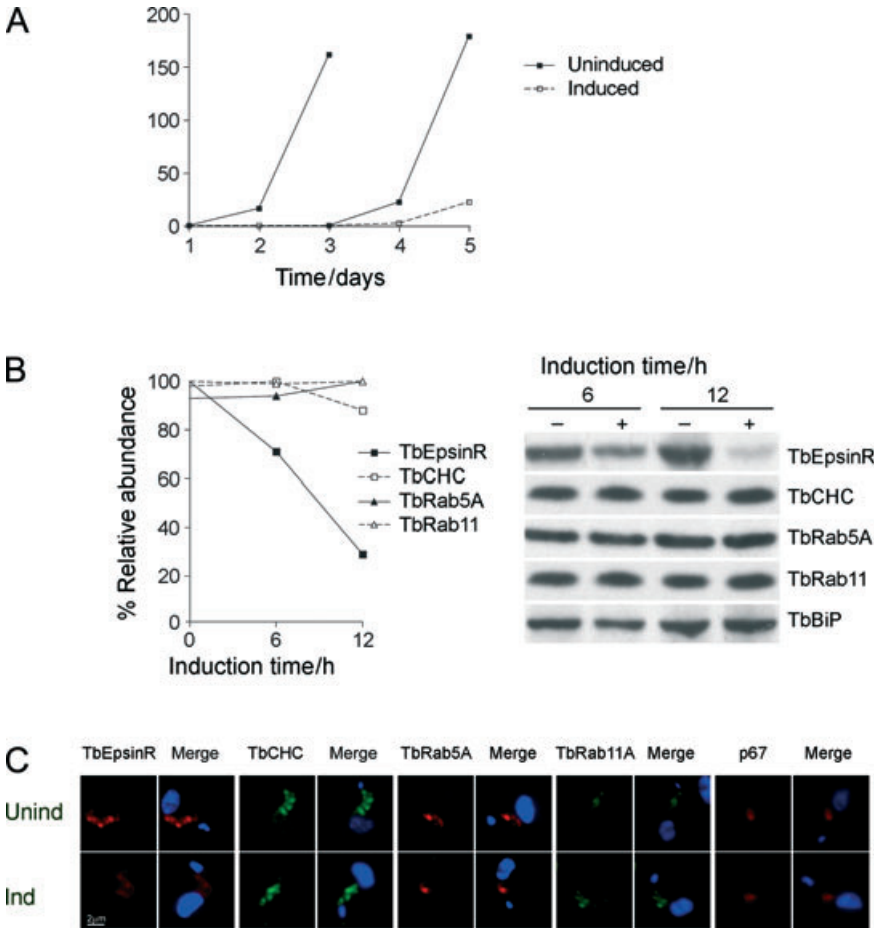

Figure 8: TbEpsinR expression is required for growth. Panel A: Growth curves for bloodstream trypanosomes transformed with p2T7TbEpsinR RNAi plasmid. Cell cultures were grown in triplicate in the presence (open squares) or absence (closed squares) of 1 μg mL^{-1} tetracycline and maintained under mid-logarithmic growth conditions by periodic dilution (indicated by breaks in the growth curves). Cell density was assessed by Coulter Counter. Data points are mean values. Panel B: Aliquots of induced and non-induced cultures were taken at the indicated times and analyzed by western blot. A decrease in TbEpsinR protein levels can be observed at an early time (6 h) and by 12 h, protein levels are reduced to <30% when compared to the non-induced control. No significant change to protein levels of the endocytic markers TbRab5A, TbCLH, the recycling endosome marker TbRab11A or the ER marker TbBiP could be detected. Quantitation of WB data is shown on the left. Panel C: Immunofluorescence analysis of endocytic factors under the same conditions as in panel B indicates that there are no major structural alterations of these membrane domains. TbEpsinR, TbRab5A and p67 in red, TbCLH and TbRab11 in green. Cells were counterstained with DAPI to visualize the nucleus and kinetoplast. Bars, 2 μM.

Immunofluorescence-based quantitation of TfR, ISG65 and ISG75 in TbEpsinR RNAi induced permeabilized cells shows that depletion of TbEpsinR caused a significant decrease to the intracellular pool of TfR, ISG65 and ISG75 (Figure 9A). No mislocalization was observed for any of the markers studied (Figure 9A). The decrease in intracellular levels was quantitated by single cell analysis; intracellular levels of the GPI-anchored TfR were reduced by ~60% in induced cells and by ~40% for the *trans*-membrane antigens ISG65 and ISG75 (Figure 9C). To ensure that this effect was not due to decreased synthesis of the antigens western blot analysis of whole lysates was also performed. No major variations in total protein levels of TfR, VSG, ISG65 or ISG75 were obtained upon knock down of TbEpsinR, while TbEpsinR itself was clearly decreased (Figure 9B). Quantitation confirmed this result, with a small protection of TfR, ISG65 and ISG75 observed, also consistent with prevention of uptake (Figure 9C). A small decrease to VSG levels was not consistently observed, and may be due to toxicity of the TbEpsinR knockdown or other effects and was not investigated further. The decrease in the intracellular pool of these surface antigens, both GPI-anchored and *trans*-membrane domain anchored, is similar to that seen for ISG65 and ISG75 intracellular levels when clathrin is knocked down (26). Hence, these data clearly support a role of TbEpsinR in endocytosis of surface proteins, but as flagellar pocket morphology remains normal without obvious effects on bulk membrane internalization.

Finally, as VSG is the overwhelming mannose-containing surface protein of trypanosomes we monitored VSG endocytosis by ConA accumulation together with receptor-mediated endocytosis by accumulation of transferrin. Fluorescence microscopy clearly showed that accumulation of FITC-ConA was compromised by TbEpsinR knockdown (Figure 10A). No mislocalization of ConA was observed, again indicating no major defects in the endomembrane system morphology. Some traffic to late endosomes/lysosomes is observed; these findings are distinct to the effects obtained for clathrin knockdown, but consistent with previous studies in mammalian cells where epsinR suppression does not lead to missorting of lysosomal enzymes (33) and cathepsin D trafficking is only impaired upon epsinR overexpression (13).

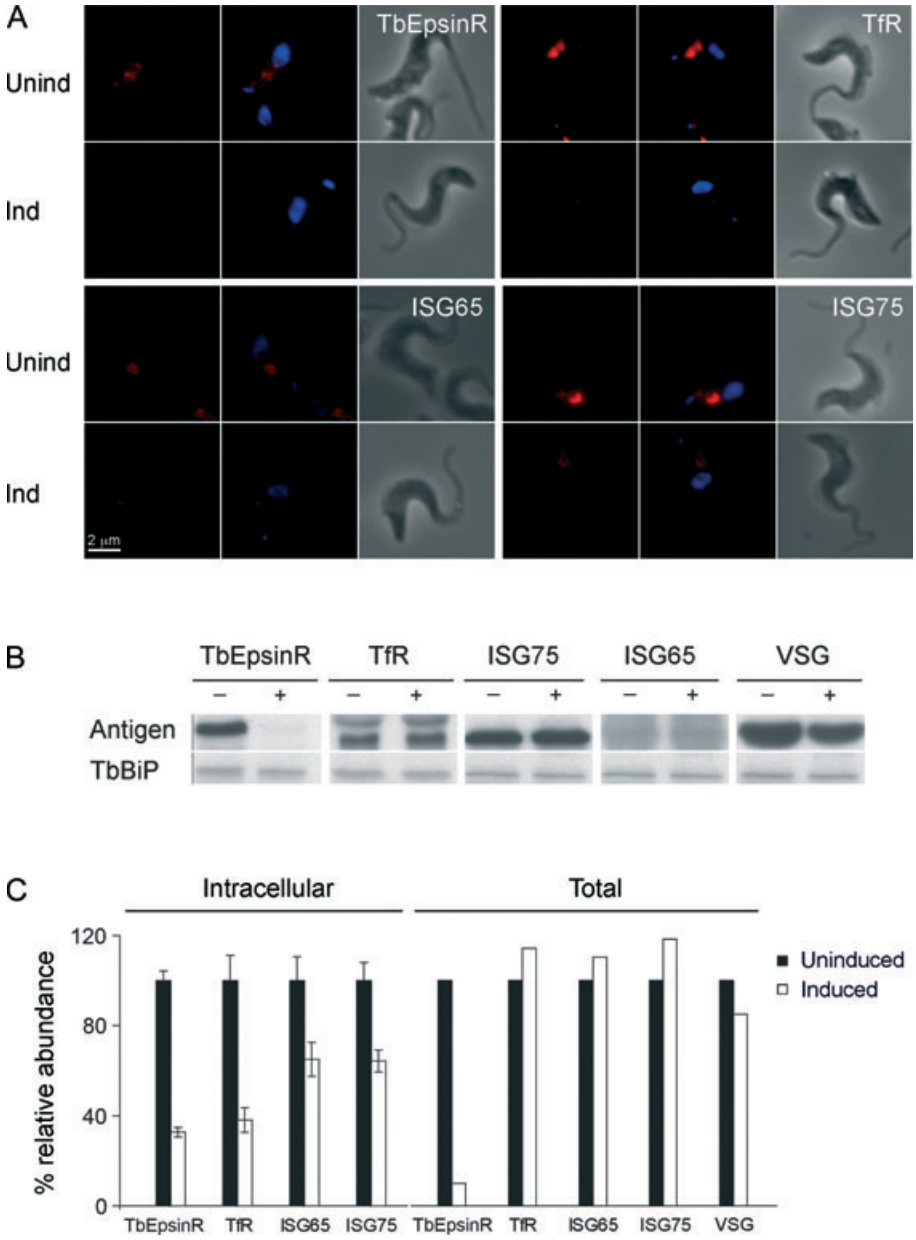

Figure 9: TbEpsinR is required for endocytosis of multiple surface proteins. Panel A: Immunofluorescence analysis of the transferrin receptor (TfR), ISG65 and ISG75 in TbEpsinR RNAi cells. Cells were induced with 1 μg mL^{-1} tetracycline for 24 h and then fixed and labeled with antibodies against the indicated markers. For each panel antigen is red, DAPI (DNA) is blue. Note that no mislocalization of the intracellular pool was observed for any of the antigens studied, but that the level of protein detected was significantly decreased. Panel B: western analysis of total protein for the above antigens in uninduced (–) and induced (+) RNAi cells under the same conditions as in panel A. TbBiP is used as a loading control. Panel C: Histograms show quantitation of intracellular fluorescence (left) and total protein abundance (right) from the analyses in panels A and B and additional replicates. Filled bars are uninduced and open bars are the induced cell levels. Immunofluorescence values are expressed in percentage of induced to uninduced conditions and represent mean values from at least 30 cells. ImageJ was used for western blot quantitation and reproducibility was confirmed in two independent experiments. Bars, 2 μM.

We used fluorescence-activated cell sorter (FACS) analysis to quantitate accumulation of both FITC-ConA and Alexa633-Tf in large numbers of cells, and also separated the data for interphase and post S-phase cells based on Hoechst staining. Uptake of both markers was reduced by approximately 50% in the induced cells when compared to the non-induced cultures. The observed endocytosis defect was similar in interphase and post-mitotic cells suggesting that the impairment in uptake was not cell–cycle-dependent (Figure 10B).

Discussion

The basic configuration of the endomembrane system appears to be very ancient and predates establishment of the major eukaryote lineages (43). Major organellar categories, including the ER, Golgi apparatus, endosomes, (MVBs) and the lysosome/vacuole all appear to have been present in the last common eukaryotic ancestor (LCEA) (20,21,43,44). This remarkable level of early sophistication in eukaryote evolution also extends to multiple molecular systems, encompassing the core fusion machinery (45,46), coat proteins (47) and trafficking of ubiquitylated cargo (26). In contrast, several aspects of the endocytic system were probably simpler in the ancestral eukaryote (47), while examples of lineage-specific features are now known, including multiple clathrin-independent endocytic pathways, features of

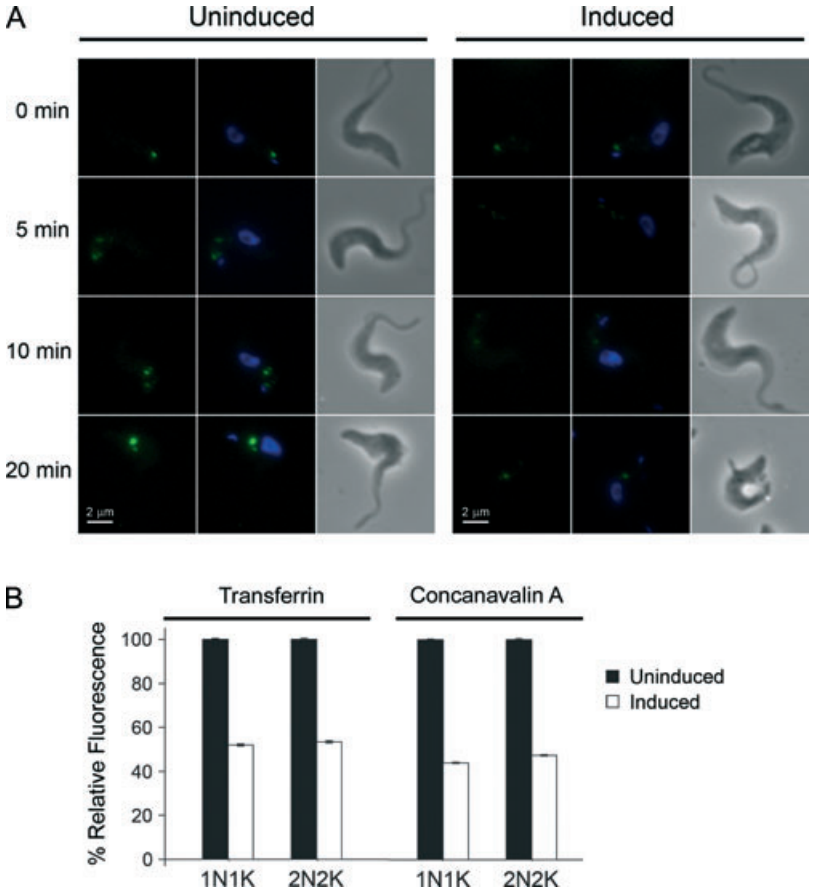

Figure 10: Receptor-mediated endocytosis is dependent on TbEpsinR RNAi. Panel A: Induced and non-induced bloodstream TbEpsinR RNAi cells were incubated with ConA at 37°C for the indicated periods prior to quenching on ice and further processing for fluorescence microscopy. In the uninduced cells, at 0 min, most of the ConA is at the flagellar pocket, at 5 min some staining of endomembrane compartments can be observed, the fluorescence distribution is more extensive at 10 min. By 20 min, cells present a strong staining of the lysosome due to accumulation of ConA in this compartment. In the induced cells, the path followed by endocytosed ConA is similar to the one observed for the non-induced culture but the labeling intensity is much reduced. Note that the major mannose-bearing structure, i.e. ConA-binding ligand, at the cell surface is VSG. Panel B: Flow cytometric analysis of ConA and transferrin uptake. BSF parasites were incubated with Alexa633-transferrin or FITC-Concanavalin A at 37°C, for the indicated period of time. Samples were quenched by adding ice-cold PBS, 3 μg mL^{-1} Hoechst to stain DNA and taken for FACS analysis. Data for each marker are presented as histograms of Transferrin uptake (left) and ConA uptake (right) in the 1K1N and 2K2N populations, at an incubation time 20 min. Relative fluorescence median values were used to calculate percent of ligand uptake. Relative fluorescence values for non-induced were set to 100% and fluorescence values for the induced cells were normalized to these values. Error bars represent the standard error of the fluorescence distribution. Bars, 2 μM.

the MVB/ESCRT system and other lineage-specific elaborations (20,21,48). The presence of lineage-specific features was suggested earlier by us for the epsin ENTH domain-containing family of proteins, where preliminary analysis indicated that higher eukaryotes possessed true UIM-containing epsins but other lineages do not (20).

The ENTH domain is highly conserved, where it is present along with binding motifs for clathrin and adaptins, suggesting an ancient role for the ENTH domain in clathrin-mediated transport. Most studies on ENTH domain proteins have focused on higher eukaryotes where two types coexist, epsin, with a role in endocytosis (9) and epsinR, principally involved in retrograde and TGN transport (13). We find that the major innovations to epsins are ubiquitin interacting motifs (UIMs) downstream of the ENTH domain that participate in endocytosis of ubiquitylated cargo (11) and NPF sequences that bind to Eps15 homology (EH) domains occurring in factors affecting actin dynamics (9,10,32,49). Apart from the presence of NPF motifs in a few non-opisthokont epsins, these domain architectures are absent from ENTH-domain proteins outside of the Opisthokonta. Further, in these taxa, ENTH-domain protein genes exist mainly as single copy. These findings are in agreement with previous analyses showing that components of the clathrin network linking endocytosis to actin dynamics and sorting of ubiquitylated cargo in metazoans and fungi are not fully conserved with the remaining eukaryotes (50).

These observations indicate a simple evolutionary history for the ENTH-domain family. The most parsimonious view is that the ancestral eukaryote had a single gene encoding an epsinR-like factor. This gene expanded in a few lineages, for example, *A. thaliana* (51) and opisthokonts, and may be partly, but not exclusively, associated with multicellularity and tissue differentiation. This pattern is reminiscent of that seen for three other endocytic-specific membrane-trafficking family paralogues (Rab5, the endocytic anterograde syntaxins and the β-subunit of AP1 and AP2). Epsin and epsinR likely represent a fourth example of a protein associated with the endocytic system that was simpler in the LCEA and that gained complexity in parallel in multiple lineages (47). A single

gene duplication event early in the opisthokont lineage, for example, allowed acquisition of the UIM by one of the resulting paralogues, and hence diversification of function. Significantly this appears to be a unique event, while expansion of the resulting epsin and epsinR genes is more common and there are multiple genes in metazoan and yeast genomes. As essentially all studies have been in opisthokonts, and epsin/epsinR have coevolved for hundreds of millions of years, the modern functions of epsinR are unlikely to reflect the ancestral roles. We used trypanosomes, which only ever possessed epsinR, to uncover the roles that epsinR plays in intracellular transport in non-Opisthokonta.

TbEpsinR has a localization characteristic of both epsin and epsinR adaptors. In mammalian cells epsin and epsinR are present within two distinct pools; epsin associates with clathrin at the plasma membrane and epsinR colocalizes with a perinuclear clathrin population (10). TbEpsinR is present at the flagellar pocket, superposes with early endocytic compartments, is in close juxtaposition to the Golgi complex but is absent from lysosomes and MVBs. TbEpsinR is intimately associated with clathrin, colocalizes with GFP-tagged CLC, is present in clathrin-coated pits at the flagellar pocket and can be isolated in a complex with clathrin by coimmunoprecipitation. TbEpsinR contains a putative clathrin-binding box that, as in *H. sapiens* epsinR, overlaps with one of the DxF adaptin-binding motifs near the carboxy terminus; the presence of clathrin-binding motifs in TbEpsinR suggests that the interaction is direct. TbEpsinR is not found associated with the exocytic carrier cisternae that are part of the Rab11 recycling system (35).

Based primarily on *in vitro* studies the distributions of epsin and epsinR are believed to be determined partly by recognition of PtdIns(4,5)P2 at the plasma membrane by epsin and PtdIns(3,5)P or PtdIns(4)P by *Saccharomyces cerevisiae (S. cerevisiae)* or mammalian epsinR respectively at intracellular compartments ((10,33,52), reviewed in (53)). At these sites both factors act by inducing membrane curvature and clathrin assembly (52,54). However, clathrin and adaptor appendage-binding motifs are also present in both *H. sapiens* epsin and epsinR (10,52), and these additional interactions are likely to contribute to subcellular localization. Basic residues along the first four helices of the ENTH domain co-ordinate binding to phospholipids (52). Conserved changes in these residues and variations in their positions within the ENTH domain in TbEpsinR compared to *H. sapiens* epsin and epsinR suggest differences in affinity of TbEpsinR for membrane phospholipids.

TbEpsinR recruitment to membranes was lost by suppression of TbCLH, and the protein redistributed from endocytic puncta to diffuse staining, indicating that targeting requires clathrin. The near complete overlap between clathrin and TbEpsinR locations suggests that the TbEpsinR-clathrin interaction is a dominant targeting mechanism, and certainly, as there is a single epsin family protein, differential targeting is impossible. However, it is also apparent that PtdIns levels are important in TbEpsinR membrane association, as knockdown of TbRab5A and TbPI4KIII-β (36,38,41) lead to significantly increased recruitment of TbEpsinR to endosomal membranes. Taken together these data indicate that PtdInsP composition of trypanosomal endosomal membranes can modulate TbEpsinR recruitment. While this cannot contribute to differential targeting, our findings demonstrate that the ancestral ENTH domain likely retains the ability to recognize specific membranes based on PtdInsP composition.

In terms of function, TbEpsinR clearly contributes to endocytosis, and participates in the uptake of multiple surface factors, including GPI-anchored and *trans*-membrane proteins. Significantly this also includes the superabundant VSG and proteins with a more modest copy number. Knockdown however, despite being lethal, did not result in an enlarged flagellar pocket in the vast majority of cells, but did produce cell-cycle defects. It is most probable that the broad effects on protein endocytosis contribute to both the lethality and cell-cycle perturbation, by considerable mistargeting of multiple factors. Similar defects have been observed for other endocytic factors in trypanosomes (55).

Epsin family adaptors are proposed to bridge the membrane and clathrin coat, based on direct interaction with clathrin and the ability of epsin adaptors to promote clathrin assembly (52,54). Live cell imaging of endocytic coat assembly indicates that clathrin precedes epsin recruitment (39,56). TbEpsinR cellular distribution is dependent on clathrin expression but no effect on clathrin localization is observed upon TbEpsinR knockdown, consistent with this view. While we cannot rule out a role for TbEpsinR in clathrin polymerization, which may in part explain the role of TbEpsinR in endocytosis, the absence of clathrin mislocalization or an enlarged flagellar pocket is strong evidence that TbEpsinR is not essential for clathrin assembly.

Fungi and animals possess several factors absent from non-opisthokont taxa, including the GGAs, caveolin, several ESCRT components and numerous additional factors (20,43). Trypanosomes also lack AP-2, and endocytosis is independent of dynamin; the former is a unique feature and potentially reflects unusual aspects of the trypanosome surface (29,57). The absence of GGAs is significant as this interaction is important to specific targeting of epsinR to the TGN; the absence of this interaction suggests that this is a derived characteristic that was absent from the LCEA. Actin also participates in trypanosome endocytosis (50) and the absence of an enlarged flagellar pocket in TbEpsinR knockdown cells is distinct to both clathrin and actin RNAi phenotypes (27,50). This suggests that TbEpsinR is not responsible for bulk flow of endocytic membrane and suggests that TbEpsinR must act downstream of actin and clathrin.

However, it is significant that in metazoa and fungi the role of epsin or epsinR in bulk flow has not been assessed as studies used exclusively protein markers and ligands and hence the importance of epsin/epsinR in lipid flow remains unknown. Further, while PtdInsP specificity is suggested to contribute to membrane targeting, in the ancestral eukaryote this was presumably less precise as the need to discriminate between epsin and epsinR was not present. Evolution of additional specificity likely accompanied differentiation between these two isoforms and differences in PtdInsP specificity detected in several species (53) may be the result of lineage-specific divergence.

How does the function of TbEpsinR compare to epsin family proteins from other systems? There is clear evidence for functional discrimination between epsin and epsinR in Opisthokonts. In yeasts, there are several epsin family genes; Ent1p and Ent2p are true epsins and are clearly implicated in endocytosis (12) and also bind ubiquitin (58). By contrast *S. cerevisiae* Ent3p and Ent5p are assigned as epsinR, locate to the Golgi complex and bind GGA adaptins (32,59). These pairs of gene products are partially redundant as, for example, Ent3 and Ent5 are synthetic lethal, but single knockouts viable (59). This functional pattern is conserved with metazoa, and epsin is a player in clathrin-mediated endocytosis, but epsinR intimately associated with *trans*-Golgi events (60); association with distinct adaptin complexes has also been reported for both epsin and epsinR, specific binding to GGA for epsinR (61), and a lack of association with caveolin, suggesting that epsins are indeed restricted in function to clathrin-dependent pathways (11), which may be the only endocytic pathway present in non-opisthokonts. However, epsinR in *Drosophila melanogaster* is essential, whereas epsin, which is required for both Delta and Notch signaling and hence implicated in endocytosis, is not an essential gene (reviewed in (62)). Significantly, a role for epsinR in Golgi-mediated trafficking is supported for *Arabidopis thaliana*, which lacks epsin. There are potentially three epsinR proteins in *A. thaliana*, two of which locate at the TGN (15). However, while AtEpsinR1 has a clear role in TGN to vacuole transport (14), AtEpsinR2 also binds AP-2, suggesting a role in endocytosis. Moreover, only a minor proportion of AtEpsinR2 is located at the Golgi complex and the majority appears associated with an as yet undefined compartment. The contribution of AtEpsinR2 to clathrin-mediated endocytosis has not been described.

Overall, our data suggest the major function of TbEpsinR is as an adaptor in clathrin-mediated endocytosis. While we are unable to assess the contribution of TbEpsinR in TGN-mediated trafficking directly due to the absence of sensitive assays or markers, the absence of effects on the lysosomal protein p67 are suggestive that any such role is minor, and is unlike the disruption observed in *S. cerevisiae* (32). We suggest that opisthokonts have increased their emphasis on ubiquitylation as a mechanism for endocytosis, consistent with the expansion of distinct endocytic pathways described for mammalian cells. Clearly, acquisition of the UIM by epsin would recruit this factor into the endocytic pathway, and provide increased scope for modulation of clathrin-mediated transport. This is consistent with the evidence here that the ancestral role for the ENTH-domain proteins was likely in endocytosis, and subsequent evolution has served to elaborate this family within the higher eukaryotes into two distinct families with differing roles.

Materials and Methods

Bioinformatics

ENTH-containing proteins were identified by BLAST analysis of complete genome databases of representative taxa in five of the six major eukaryotic supergroups using *S. cerevisiae* and metazoan sequences as initial queries (63). No complete genome database for a representative Rhizarian (the sixth supergroup) was available. *T. brucei, Plasmodium falciparum (P. falciparum), Entamoeba histolytica (E. histolytica)* and *Dictyostelium discoideum (D. discoideum)* data were obtained from geneDB (www.genedb.org). *Thalassiosira pseudonana (T. pseudonana), Phytophthora ramorum (P. ramorum), Ostreococcus tauri (O. tauri), Naegleria gruberi (N. gruberi), Chlamydomonas reinhardtii (C. reinhardtii)* and *Ciona intestinalis (C. intestinals)* data were from the joint genome initiative (genome.jgi-psf.org). *Trichomonas vaginalis (T. vaginalis), Tetrahymena thermophila (T. thermophila), Theileria parva (T. parva), Cryptococcus neoformans (C. neoformans)* and *A. thaliana* data were from TIGR (www.tigr.org). *Giardia lamblia (G. lamblia)* data were obtained from GiardiaDB (www.mbl.edu/Giardia), *Toxoplasma gondii (T. gondii)* data from ToxoDB (www.toxodb.org), *Cryptosporidium parvum (C. parvum)* data from CryptoDB (www.cryptodb.org) and *Cyanidioschyzon merolae (C. merolae)* data were retrieved from the *C. merolae* genome BLAST server (merolae.biol.s.u-tokyo.ac.jp). Fungal data was obtained from the Munich Information Center for Protein Sequences (MIPS) database (mips.gsf.de) and *Drosophila melanogaster* data was at FlyBase (www.flybase.org). All remaining genomic data were retrieved through National Center for Biotechnology Information (NCBI) (blast.ncbi.nlm.nih.gov/Blast.cgi). This procedure identified Tb11.50.0006 as an ENTH-domain protein, and the sole representative in *T. brucei*. Retrieved sequences were aligned using MUltiple Sequence Comparison by Log-Expectation (MUSCLE) (64) and adjusted by eye. Only regions of unambiguous homology were retained for phylogenetic analysis.

An initial alignment contained all 49 sequences collected. Long branches, i.e. divergent sequences, were identified in the initial tree topology and from the presence of regions incongruous with the overall alignment, including non-canonical features within the ENTH domain. A sub-dataset, with these divergent data removed, contained 35 sequences but retained representatives from all five eukaryotic supergroups (63). Prot-test 1.3 (65) was used to select the appropriate model of sequence evolution in both cases; for the initial dataset a Whelan and Goldman (WAG) model (66) plus a gamma (G) correction of 2.62 was used, while for the second dataset a WAG + I (0.01) + G (2.62) model was applied. Phylogenetic analysis was performed using MrBayes Version 3.1.2 (10^6 generations) (67) and PhyML (68) and RAxML (69) (100 pseudoreplicates). All alignments are available upon request.

Cell lines and propagation

T. brucei BSF and procyclic form (PCF) Lister 427 laboratory-adapted strains were cultured in HMI9 and SDM79 media respectively supplemented with 10% fetal bovine serum as described previously (70). For RNA interference experiments, the tetracycline-responsive single marker bloodstream-form

(SMB) cell line was cultured as described (40). BSF cells expressing GRASP-GFP were maintained in the presence of 2.5 μg mL^{-1} geneticin. The genomic-tagged CLC-GFP cell line was maintained in the presence of 0.2 μg mL^{-1} puromycin.

RNA interference

A 438bp fragment of Tb11.50.0006 was selected and verified by RNAit software to specifically target the gene product in RNAi experiments (71). This fragment was PCR-amplified from *T. brucei* genomic DNA using specific primers (FOR, GGCCAAATTGAGTGGTGAG; REV, CTAGGCTCTGCCTTTGGATG) and inserted into the $p2T7^{TABlue}$ plasmid. An AMAXA nucleofector was used to transfect tetracycline-responsive log-phase SMB with *NotI* digested p2T7- TbEpsinR following the manufacturer's procedure and as previously described (28). Single clones were selected and maintained in the presence of 5 μg mL^{-1} hygromycin and 2.5 μg mL^{-1} geneticin. To generate the TbPI4KIII-β RNAi cell line a fragment of Tb927.4.1140 (37) was cloned into $p2T7^{TABlue}$ plasmid and SMB cells were transfected as described earlier. TbCLH RNAi and TbRab5A RNAi were as described previously (27,41). For growth curves, cultures were inoculated to a concentration of 10^4 cells mL^{-1} in triplicate with or without tetracycline at 1 μg mL^{-1}. To monitor cell numbers cell density was assessed using a Z2 Coulter Counter (Beckman).

Antibodies

The full-length TbEpsinR ORF was amplified from *T. brucei* genomic DNA using the selected primers; FOR, ACTTGGATCCATGTCATTTCCGACTTCTC and REV, AGTGGATCCCTACTGACCTAACCGGCGACC, and cloned downstream and in frame with GST into the BamHI site of pGEX6P. GST-TbEpsinR was expressed in BL21(DE3) transformed *E. coli* with pGEX6P. TbEpsinR in L-broth and induced with 1.0 mM isopropyl-β-D-thiogalactopyranoside. Recombinant protein was affinity purified on glutathione-sepharose-4B (GE Healthcare) according to the manufacturer's procedure. Purity of isolated GST-TbEpsinR was estimated at ~95% by SDS-PAGE and Coomassie Blue staining. Protein yield was quantitated by $OD_{280\ nm}$ at ~2 mg L^{-1}. TbEpsinR antiserum was raised in rabbits against the full-length fusion protein; rabbits were immunized four times with a total of 2 mg recombinant protein in Freund's complete adjuvant (Covalab). For antibody affinity purification, GST-TbEpsinR was immobilized on cyanogen bromide-activated agarose (Sigma) following the manufacturer's procedure and antibody purified by standard procedures. Anti-TbEpsinR purified antibody was stored in 50% glycerol/PBS at −20°C. The purified antibody was tested by western blotting and competition assays using excess soluble GST-TbEpsinR confirmed the antibody to be specific (Figure S2). Monoclonal Mab280 to the lysosomal protein p67 and rabbit anti-TbBiP antibodies were a gift of James D. Bangs (University of Wisconsin, Madison), affinity-purified anti-221 VSG, anti-ISG75 and anti-ISG65 antibodies were a gift of Mark Carrington (University of Cambridge), anti-transferrin receptor was a gift of Piet Borst (The Netherlands Cancer Institute, Amsterdam), mouse anti-TbRab11A and rabbit anti-TbRab5A, anti-TbRab11A and anti-TbCLH antibodies were as described previously (72–74).

Protein electrophoresis and western blotting

For western analysis lysates of 10^6–10^7 trypanosome cells per lane were separated by 12% SDS-PAGE and transferred onto ImmobilonP (Millipore). Membranes were blocked and processed following standard procedures. The rabbit polyclonal TbEpsinR, TbRab5A and TbRab11A antibodies were used at a dilution of 1:2000. All the other antibodies were at 1:10 000. Detection used enhanced chemiluminescence and exposure to X-ray film. Films were scanned and exposures quantitated using ImageJ software (NIH); data are expressed in arbitrary units and normalized to TbBiP, following reprobing, as a loading control.

Immunoelectron microscopy

Cells were fixed with 4% paraformaldehyde (PFA) and 0.05% glutaraldehyde in PBS buffer on ice for an hour and washed with PBS. The cells were incubated in 0.1M PIPES buffer containing 5% BSA and 20% polypropylene glycol, concentrated by centrifugation at 800 g (Hermle Z 160 M, Hermle Laboratecnic) and the supernatant was removed. Small droplets (5 μL) of the cells were mounted onto aluminium foil and quench frozen, by plunging them into melting propane cooled in liquid nitrogen. After freezing the cells were transferred into a Leica automatic freeze substitution apparatus (AFS) freeze substitution unit (Leica) in vials of frozen, dry methanol, containing 0.5% uranyl acetate. They were maintained at −90°C for 24 h followed by 24 h at −70°C and another 24 h at −50°C. They were infiltrated with Lowicryl HM20 over 3 days and polymerized by irradiation with ultraviolet (UV) light for 48 h. Thin sections were cut using a Leica Ultracut S (Leica) and mounted on Formvar coated nickel grids. The sections were incubated overnight in rabbit anti-TbEpsinR primary antibodies, diluted 1:50 in PBS at pH 7.4 containing 0.001% Tween-20, 0.001% Triton-X-100, 2% BSA. They were washed four times in PBS and incubated with goat anti-rabbit immunoglobulins conjugated to 10 nm gold particles (British Biocell, GB), diluted 1:200 in the diluent for the primary antibody for 1 h (75). They were rinsed four times in PBS and twice in deionized water and stained with uranyl acetate and lead citrate before viewing in a Philips CM100 (FEI-Philips) transmission EM.

Immunofluorescence

Cells were grown to log-phase, fixed in 3% paraformaldehyde (PFA) in Voorheis's modified PBS (vPBS) and adhered to poly-L-lysine slides (Sigma). For immunostaining, cells were permeabilized with 0.1% Triton-X-100 and blocked in foetal bovine serum. Slides were incubated with antibodies as described previously (76) and mounted with Vectashield containing DAPI to stain DNA (Vectalabs). Primary antibody working dilutions were 1:500 for rabbit anti-TbEpsinR, 1:250 for TbRab5A and TbRab11A, and 1:1000 for all other antibodies. Cells were examined on Nikon Eclipse 400 epifluorescence microscope fitted with a Hamamatsu CCD digital camera. Image acquisition was performed with Metamorph software (Molecular Devices, Version 6) and processing in Photoshop (Adobe). All quantitation was done using identical exposures as appropriate and using the raw data within Metamorph. Subsequent image processing for presentation purposes only was performed with Photoshop.

Incubation with wortmannin

BSF cells were treated with wortmannin at a final concentration of 30 μM for 60 min in DMSO and further processed for immunostaining with anti-TbEpsinR antibody as described earlier.

Concanavalin A staining of flagellar pocket and endomembrane compartments

Bloodstream parasites were grown to log-phase and washed once with serum-free HMI-9 medium supplemented with 1% BSA, cells were then resuspended to a density of 10^7 cells mL^{-1} and incubated in this media at 4°C or 12°C for 20 min. FITC-conjugated ConA was added to a final concentration of 0.1 mg mL^{-1} (Vectalabs) and cells were incubated at these temperatures for another 20 min to label flagellar pocket or early endosomes. FITC-ConA uptake was stopped by placing the cells on ice prior to processing further for immunofluorescence as described earlier.

Anti-TbEpsinR immunoprecipitation

BSF cells were harvested by centrifugation, washed with PBS and resuspended with lysis buffer [20 mM Hepes-KOH, pH 7.5, 110 mM KAc, 75 mM NaCl, 0.1% NP40 and complete protease inhibitor cocktail (Roche)] and centrifuged in a microfuge at 16 000 g for 10 min, 4°C. Anti-TbEpsinR, anti-CLH, or anti-BiP were added to aliquots of the cell lysates and incubated for 2 h at 4°C. Immune complexes were isolated by incubating with 20 μL of protein A Sepharose beads for 1 h at 4°C. The beads were washed five times with ice-cold lysis buffer, resuspended in 1xSDS-PAGE loading buffer and boiled for 5 min. Samples were subjected to western blot analysis as described earlier.

Subcellular fractionation

Cells were grown to logarithmic phase and washed twice in PBS, resuspended in cold hypotonic lysis buffer (10 mM TRIS-HCl, pH 7.5 plus protease inhibitors) and then incubated on ice for 5 min. The cell lysate was centrifuged in a refrigerate microfuge at 16 000 g at 4°C for 10 min. The pellet fraction was washed once with cold hypotonic lysis buffer, resuspended in sample buffer and incubated on ice for 25 min prior to taking for SDS-PAGE. Equivalent amounts of SN, wash and pellet fractions were analyzed by western blotting.

Analysis of Concanavalin A and transferrin endocytosis

Cells containing the p2T7-TbEpsinR RNAi plasmid were grown to logarithmic phase and induced for 24 h. Control cultures were uninduced. Cells were then washed and resuspended in serum-free HMI-9/1% BSA to a final concentration of 10^7 cells mL^{-1}. Aliquots of washed cells were then transferred to a 37°C incubator and equilibrated for 20 min. ConA-fluorescein or transferrin-Alexa Fluor 633 conjugate (Molecular Probes) were added to a concentration of 5 $\mu g\ mL^{-1}$ or 25 $\mu g\ mL^{-1}$ respectively. At 0, 5, 10 and 20 min, 1 mL aliquots were withdrawn and added to ice-cold PBS to prevent further ligand uptake. Cells were washed thoroughly to remove excess fluor, and resuspended in PBS with Hoechst to stain DNA. Cells were fixed in 1% formaldehyde and analyzed. Cell-associated fluorescence from 30 000 to 50 000 cells was measured for fluorescein at 530/540 nm or Alexa633 at 665/720 nm using Cyan ADP (DakoCytomation). Data were analyzed with Summit software (Cytomation). All fluorescence data was scaled using log amplifiers except for cell-cycle data where linear amplifiers were used. Amplifier gains were adjusted to untreated cells to control for autofluorescence.

Acknowledgments

This work was supported by a program grant from the Wellcome Trust (to MCF), and benefited from equipment support through CamPOD. JBD was supported by fellowships from the Parke-Davis Foundation and the Wellcome Trust. ImmunoEM data were gathered at the Multi-imaging Unit, University of Cambridge, with thanks to Jeremy Skepper, while phylogenetic analyses were performed using the CamGrid computational resource. We thank James Bangs (Madison) and Mark Carrington (Cambridge) for antibodies, Senthil Natesan (Cambridge) for the GFP-tagged clathrin-light chain trypanosomes and Graham Warren (Vienna) for the GRASP-GFP construct. We also thank Markus Engstler (Würzburg) for discussions.

Supporting Information

Additional Supporting Information may be found in the online version of this article:

Figure S1: Phylogenetic analysis of Epsin/EpsinR families. The topologies generated from three different algorithms are shown. A) MrBayes, B) RaxML and C) PhyML. In each case numbers against the internodes indicate statistical support, either posterior probability (A) or bootstrap values (B and C).

Figure S2: TbEpsinR antibody verification. BSF cell lysate and purified recombinant GST-TbEpsinR from *E.coli* were fractionated by SDS-PAGE in duplicate, and analyzed by western blotting with anti-TbEpsinR antibody (left panels), or anti-TbEpsinR antibody pre-incubated with recombinant purified GST-TbEpsinR (right panels). Note that the signal is lost when the antibody is pre-incubated with the recombinant protein.

Figure S3: Absence of morphological abnormalities following TbRab5A RNAi. Cells were induced for RNAi of TbRab5A as described in *Methods*. Cells were prepared for thin section transmission EM as described (27). Scale bars are 2 um (panel A) and 5 um (panels B–D). Apart from the apparent compression of internal membrane-bound compartments, there is no evidence for proliferation, enlargement or other abnormal endosomal structures under these conditions.

Figure S4: TbEpsinR expression levels in TbRab5A RNAi cells. TbRab5A RNAi was induded in cells with 1 $\mu g\ mL^{-1}$ tetracycline for 24 h and whole cell lysates analyzed by western blotting for TbEpsinR and TbRab5A. TbBiP was used as a loading control. Histograms show quantitation of total protein, filled bars are expression levels in uninduced cells and open bars are expression levels in induced cells.

Figure S5: Cell-cycle analysis of TbEpsinR knockdown cells. p2T7-TbEpsinR cells were induced for 24 h with tetracycline, fixed with 4% paraformaldehyde and stained with DAPI. Panel A: To determine position in the cell-cycle, the numbers of nuclei and kinetoplasts per cell were counted for at least 200 cells for uninduced and induced cultures. Panel B: Light microscopy was used to determine incidence of cells with abnormal morphologies and cells presenting the Big Eye phenotype; at least 200 cells were counted.

Figure S6: TbEpsinR protein copy number. Lysates of 10^7 BSF cells, and aliquots of purified GST-TbEpsinR equivalent to 10^{11}, 10^{12} and 10^{13} copies of recombinant protein, estimated based on protein concentration, were analyzed by western blotting with anti-TbEpsinR antibody. The TbEpsinR copy number in BSF was estimated to be between 10^4 and 10^5 copies per cell.

Table S1: Accessions for Epsin and EpsinR candidates retrieved from various databases and as used in the phylogenetic analysis (see *Methods* for sources of these data).

Please note: Wiley-Blackwell are not responsible for the content or functionality of any supporting materials supplied by the authors. Any queries (other than missing material) should be directed to the corresponding author for the article.

References

1. Glebov OO, Bright NA, Nichols BJ. Flotillin-1 defines a clathrin-independent endocytic pathway in mammalian cells. Nat Cell Biol 2006;8:46–54.
2. Roth AF, Davis NG. Ubiquitination of the PEST-like endocytosis signal of the yeast a-factor receptor. J Biol Chem 2000;275:8143–8153.
3. Overstreet E, Fitch E, Fischer JA. Fat facets and Liquid facets promote Delta endocytosis and Delta signaling in the signaling cells. Development 2004;131:5355–5366.
4. Tian X, Hansen D, Schedl T, Skeath JB. Epsin potentiates Notch pathway activity in *Drosophila* and *C. elegans*. Development 2004;131:5807–5815.
5. Newpher TM, Smith RP, Lemmon V, Lemmon SK. In vivo dynamics of clathrin and its adaptor-dependent recruitment to the actin-based endocytic machinery in yeast. Dev Cell 2005;9:87–98.
6. Tan PK, Howard JP, Payne GS. The sequence NPFXD defines a new class of endocytosis signal in *Saccharomyces cerevisiae*. J Cell Biol 1996;135:1789–1800.
7. Roth AF, Davis NG. Ubiquitination of the yeast a-factor receptor. J Cell Biol 1996;134:661–674.
8. Praefcke GJ, Ford MG, Schmid EM, Olesen LE, Gallop JL, Peak-Chew SY, Vallis Y, Babu MM, Mills IG, McMahon HT. Evolving nature of the AP2 alpha-appendage hub during clathrin-coated vesicle endocytosis. EMBO J 2004;23:4371–4383.

9. Chen H, Fre S, Slepnev VI, Capua MR, Takei K, Butler MH, Di Fiore PP, De Camilli P. Epsin is an EH-domain-binding protein implicated in clathrin-mediated endocytosis. Nature 1998;394:793–797.
10. Mills IG, Praefcke GJ, Vallis Y, Peter BJ, Olesen LE, Gallop JL, Butler PJ, Evans PR, McMahon HT. EpsinR: an AP1/clathrin interacting protein involved in vesicle trafficking. J Cell Biol 2003;160:213–222.
11. Hawryluk MJ, Keyel PA, Mishra SK, Watkins SC, Heuser JE, Traub LM. Epsin 1 is a polyubiquitin-selective clathrin-associated sorting protein. Traffic 2006;7:262–281.
12. Wendland B, Steece KE, Emr SD. Yeast epsins contain an essential N-terminal ENTH domain, bind clathrin and are required for endocytosis. EMBO J 1999;18:4383–4393.
13. Saint-Pol A, Yelamos B, Amessou M, Mills IG, Dugast M, Tenza D, Schu P, Antony C, McMahon HT, Lamaze C, Johannes L. Clathrin adaptor epsinR is required for retrograde sorting on early endosomal membranes. Dev Cell 2004;6:525–538.
14. Song J, Lee MH, Lee GJ, Yoo CM, Hwang I. *Arabidopsis* EPSIN1 plays an important role in vacuolar trafficking of soluble cargo proteins in plant cells via interactions with clathrin, AP-1, VTI11, and VSR1. Plant Cell 2006;18:2258–2274.
15. Lee GJ, Kim H, Kang H, Jang M, Lee DW, Lee S, Hwang I. EpsinR2 interacts with clathrin, adaptor protein-3, AtVTI12, and phosphatidylinositol-3-phosphate. Implications for EpsinR2 function in protein trafficking in plant cells. Plant Physiol 2007;143:1561–1575.
16. Chidambaram S, Mullers N, Wiederhold K, Haucke V, von Mollard GF. Specific interaction between SNAREs and epsin N-terminal homology (ENTH) domains of epsin-related proteins in trans-Golgi network to endosome transport. J Biol Chem 2004;279:4175–4179.
17. Repass SL, Brady RJ, O'Halloran TJ. *Dictyostelium* Hip1r contributes to spore shape and requires epsin for phosphorylation and localization. J Cell Sci 2007;120:3977–3988.
18. Roth MG. Integrating actin assembly and endocytosis. Dev Cell 2007;13:3–4.
19. Maldonado-Baez L, Dores MR, Perkins EM, Drivas TG, Hicke L, Wendland B. Interaction between Epsin/Yap180 adaptors and the scaffolds Ede1/Pan1 is required for endocytosis. Mol Biol Cell 2008;19:2936–2948.
20. Field MC, Gabernet-Castello C, Dacks JB. Reconstructing the evolution of the endocytic system: insights from genomics and molecular cell biology. Adv Exp Med Biol 2007;607:84–96.
21. Leung KF, Dacks JB, Field MC. Evolution of the multivesicular body ESCRT machinery; retention across the eukaryotic lineage. Traffic 2008;9:1698–1716.
22. Gouet P, Courcelle E, Stuart DI, Metoz F. ESPript: analysis of multiple sequence alignments in PostScript. Bioinformatics 1999;15:305–308.
23. Miller SE, Collins BM, McCoy AJ, Robinson MS, Owen DJ. A SNARE-adaptor interaction is a new mode of cargo recognition in clathrin-coated vesicles. Nature 2007;450:570–574.
24. Field MC, Carrington M. Intracellular membrane transport systems in *Trypanosoma brucei*. Traffic 2004;5:905–913.
25. Engstler M, Pfohl T, Herminghaus S, Boshart M, Wiegertjes G, Heddergott N, Overath P. Hydrodynamic flow-mediated protein sorting on the cell surface of trypanosomes. Cell 2007;131:505–515.
26. Chung WL, Leung KF, Carrington M, Field MC. Ubiquitylation is required for degradation of transmembrane surface proteins in trypanosomes. Traffic 2008;9:1681–1697.
27. Allen CL, Goulding D, Field MC. Clathrin-mediated endocytosis is essential in *Trypanosoma brucei*. EMBO J 2003;22:4991–5002.
28. Koumandou VL, Natesan SK, Sergeenko T, Field MC. The trypanosome transcriptome is remodelled during differentiation but displays limited responsiveness within life stages. BMC Genomics 2008;9:298.
29. Morgan GW, Hall BS, Denny PW, Field MC, Carrington M. The endocytic apparatus of the kinetoplastida. Part II: machinery and components of the system. Trends Parasitol 2002;18:540–546.
30. Brickman MJ, Balber AE. *Trypanosoma brucei rhodesiense* bloodstream forms: surface ricin-binding glycoproteins are localized exclusively in the flagellar pocket and the flagellar adhesion zone. J Protozool 1990;37:219–224.
31. Brickman MJ, Cook JM, Balber AE. Low temperature reversibly inhibits transport from tubular endosomes to a perinuclear, acidic compartment in African trypanosomes. J Cell Sci 1995;108(11):3611–3621.
32. Duncan MC, Costaguta G, Payne GS. Yeast epsin-related proteins required for Golgi-endosome traffic define a gamma-adaptin ear-binding motif. Nat Cell Biol 2003;5:77–81.
33. Hirst J, Motley A, Harasaki K, Peak Chew SY, Robinson MS. EpsinR: an ENTH domain-containing protein that interacts with AP-1. Mol Biol Cell 2003;14:625–641.
34. He CY, Ho HH, Malsam J, Chalouni C, West CM, Ullu E, Toomre D, Warren G. Golgi duplication in *Trypanosoma brucei*. J Cell Biol 2004;165:313–321.
35. Grunfelder CG, Engstler M, Weise F, Schwarz H, Stierhof YD, Morgan GW, Field MC, Overath P. Endocytosis of a glycosylphosphatidylinositol-anchored protein via clathrin-coated vesicles, sorting by default in endosomes, and exocytosis via RAB11-positive carriers. Mol Biol Cell 2003;14:2029–2040.
36. Shin HW, Hayashi M, Christoforidis S, Lacas-Gervais S, Hoepfner S, Wenk MR, Modregger J, Uttenweiler-Joseph S, Wilm M, Nystuen A, Frankel WN, Solimena M, De Camilli P, Zerial M. An enzymatic cascade of Rab5 effectors regulates phosphoinositide turnover in the endocytic pathway. J Cell Biol 2005;170:607–618.
37. Rodgers MJ, Albanesi JP, Phillips MA. Phosphatidylinositol 4-kinase III-beta is required for Golgi maintenance and cytokinesis in *Trypanosoma brucei*. Eukaryot Cell 2007;6:1108–1118.
38. Hall BS, Gabernet-Castello C, Voak A, Goulding D, Natesan SK, Field MC. TbVps34, the trypanosome orthologue of Vps34, is required for Golgi complex segregation. J Biol Chem 2006;281:27600–27612.
39. Toret CP, Lee L, Sekiya-Kawasaki M, Drubin DG. Multiple pathways regulate endocytic coat disassembly in *Saccharomyces cerevisiae* for optimal downstream trafficking. Traffic 2008;9:848–859.
40. Wirtz E, Leal S, Ochatt C, Cross GA. A tightly regulated inducible expression system for conditional gene knock-outs and dominant-negative genetics in *Trypanosoma brucei*. Mol Biochem Parasitol 1999;99:89–101.
41. Hall B, Allen CL, Goulding D, Field MC. Both of the Rab5 subfamily small GTPases of *Trypanosoma brucei* are essential and required for endocytosis. Mol Biochem Parasitol 2004;138:67–77.
42. Borst P, Fairlamb AH. Surface receptors and transporters of *Trypanosoma brucei*. Annu Rev Microbiol 1998;52:745–778.
43. Dacks JB, Field MC. Evolution of the eukaryotic membrane-trafficking system: origin, tempo and mode. J Cell Sci 2007;120:2977–2985.
44. Dacks JB, Davis LA, Sjogren AM, Andersson JO, Roger AJ, Doolittle WF. Evidence for Golgi bodies in proposed 'Golgi-lacking' lineages. Proc Biol Sci 2003;270(Suppl. 2):S168–171.
45. Pereira-Leal JB, Seabra MC. Evolution of the Rab family of small GTP-binding proteins. J Mol Biol 2001;313:889–901.
46. Koumandou VL, Dacks JB, Coulson RM, Field MC. Control systems for membrane fusion in the ancestral eukaryote; evolution of tethering complexes and SM proteins. BMC Evol Biol 2007;7:29.
47. Dacks JB, Poon PP, Field MC. Phylogeny of endocytic components yields insight into the process of nonendosymbiotic organelle evolution. Proc Natl Acad Sci U S A 2008;105:588–593.
48. Rutherford S, Moore I. The *Arabidopsis* Rab GTPase family: another enigma variation. Curr Opin Plant Biol 2002;5:518–528.
49. Aguilar RC, Watson HA, Wendland B. The yeast Epsin Ent1 is recruited to membranes through multiple independent interactions. J Biol Chem 2003;278:10737–10743.
50. Garcia-Salcedo JA, Perez-Morga D, Gijon P, Dilbeck V, Pays E, Nolan DP. A differential role for actin during the life cycle of *Trypanosoma*

brucei. EMBO J 2004;23:780–789.
51. Holstein SE, Oliviusson P. Sequence analysis of *Arabidopsis thaliana* E/ANTH-domain-containing proteins: membrane tethers of the clathrin-dependent vesicle budding machinery. Protoplasma 2005;226:13–21.
52. Ford MG, Mills IG, Peter BJ, Vallis Y, Praefcke GJ, Evans PR, McMahon HT. Curvature of clathrin-coated pits driven by epsin. Nature 2002;419:361–366.
53. Itoh T, De Camilli P. BAR, F-BAR (EFC) and ENTH/ANTH domains in the regulation of membrane-cytosol interfaces and membrane curvature. Biochim Biophys Acta 2006;1761:897–912.
54. Wasiak S, Legendre-Guillemin V, Puertollano R, Blondeau F, Girard M, de Heuvel E, Boismenu D, Bell AW, Bonifacino JS, McPherson PS. Enthoprotin: a novel clathrin-associated protein identified through subcellular proteomics. J Cell Biol 2002;158:855–862.
55. Hall BS, Smith E, Langer W, Jacobs LA, Goulding D, Field MC. Developmental variation in Rab11-dependent trafficking in *Trypanosoma brucei*. Eukaryot Cell 2005;4:971–980.
56. Kaksonen M, Toret CP, Drubin DG. A modular design for the clathrin- and actin-mediated endocytosis machinery. Cell 2005;123:305–320.
57. Morgan GW, Goulding D, Field MC. The single dynamin-like protein of *Trypanosoma brucei* regulates mitochondrial division and is not required for endocytosis. J Biol Chem 2004;279:10692–10701.
58. Shih SC, Katzmann DJ, Schnell JD, Sutanto M, Emr SD, Hicke L. Epsins and Vps27p/Hrs contain ubiquitin-binding domains that function in receptor endocytosis. Nat Cell Biol 2002;4:389–393.
59. Costaguta G, Duncan MC, Fernandez GE, Huang GH, Payne GS. Distinct roles for TGN/endosome epsin-like adaptors Ent3p and Ent5p. Mol Biol Cell 2006;17:3907–3920.
60. Kalthoff C, Alves J, Urbanke C, Knorr R, Ungewickell EJ. Unusual structural organization of the endocytic proteins AP180 and epsin 1. J Biol Chem 2002;277:8209–8216.
61. Legendre-Guillemin V, Wasiak S, Hussain NK, Angers A, McPherson PS. ENTH/ANTH proteins and clathrin-mediated membrane budding. J Cell Sci 2004;117:9–18.
62. Fischer JA, Eun SH, Doolan BT. Endocytosis, endosome trafficking, and the regulation of *Drosophila* development. Annu Rev Cell Dev Biol 2006;22:181–206.
63. Adl SM, Simpson AG, Farmer MA, Andersen RA, Anderson OR, Barta JR, Bowser SS, Brugerolle G, Fensome RA, Fredericq S, James TY, Karpov S, Kugrens P, Krug J, Lane CE et al. The new higher level classification of eukaryotes with emphasis on the taxonomy of protists. J Eukaryot Microbiol 2005;52:399–451.
64. Edgar RC. MUSCLE: multiple sequence alignment with high accuracy and high throughput. Nucleic Acids Res 2004;32:1792–1797.
65. Abascal F, Zardoya R, Posada D. ProtTest: selection of best-fit models of protein evolution. Bioinformatics 2005;21:2104–2105.
66. Whelan S, Goldman N. A general empirical model of protein evolution derived from multiple protein families using a maximum-likelihood approach. Mol Biol Evol 2001;18:691–699.
67. Ronquist F, Huelsenbeck JP. MrBayes 3: Bayesian phylogenetic inference under mixed models. Bioinformatics 2003;19:1572–1574.
68. Guindon S, Gascuel O. A simple, fast, and accurate algorithm to estimate large phylogenies by maximum likelihood. Syst Biol 2003;52:696–704.
69. Stamatakis A. RAxML-VI-HPC: maximum likelihood-based phylogenetic analyses with thousands of taxa and mixed models. Bioinformatics 2006;22:2688–2690.
70. Field H, Field MC. Tandem duplication of rab genes followed by sequence divergence and acquisition of distinct functions in *Trypanosoma brucei*. J Biol Chem 1997;272:10498–10505.
71. Redmond S, Vadivelu J, Field MC. RNAit: an automated web-based tool for the selection of RNAi targets in *Trypanosoma brucei*. Mol Biochem Parasitol 2003;128:115–118.
72. Field H, Farjah M, Pal A, Gull K, Field MC. Complexity of trypanosomatid endocytosis pathways revealed by Rab4 and Rab5 isoforms in *Trypanosoma brucei*. J Biol Chem 1998;273:32102–32110.
73. Jeffries TR, Morgan GW, Field MC. A developmentally regulated rab11 homologue in *Trypanosoma brucei* is involved in recycling processes. J Cell Sci 2001;114:2617–2626.
74. Morgan GW, Allen CL, Jeffries TR, Hollinshead M, Field MC. Developmental and morphological regulation of clathrin-mediated endocytosis in *Trypanosoma brucei*. J Cell Sci 2001;114:2605–2615.
75. Skepper JN. Immunocytochemical strategies for electron microscopy: choice or compromise. J Microsc 2000;199:1–36.
76. Field MC, Allen CL, Dhir V, Goulding D, Hall BS, Morgan GW, Veazey P, Engstler M. New approaches to the microscopic imaging of *Trypanosoma brucei*. Microsc Microanal 2004;10:621–636.